Environ. Sci. Technol. **2002**, *36,* 5335−5341

In Situ Mobilization of Colloids and Transport of Cesium in Hanford Sediments

MARKUS FLURY,*
JON B. MATHISON, AND
JAMES B. HARSH

Department of Crop and Soil Sciences, Center for Multiphase Environmental Research, Washington State University, Pullman, Washington 99164-6420

Radioactive waste, accumulated during Pu production, has leaked into the subsurface from underground storage tanks at the U.S. Department of Energy's Hanford site. The leaking solutions contained ^{137}Cs and were of high ionic strength. Such a tank leak was simulated experimentally in steady-state flow experiments with packed Hanford sediments. The initial leak was simulated by a 1 M $NaNO_3$ solution, followed by a decrease of ionic strength to 1 mM $NaNO_3$. Cesium breakthrough curves were determined in both 1 M and 1 mM $NaNO_3$ background. Colloidal particles were mobilized during the change of ionic strength. Mobilized colloids consisted mainly of quartz, mica, illite, kaolinite, and chlorite. Electrophoretic mobilities of colloids in the eluent solution were $-3(\mu m/s)(V/cm)$ and increased to less negative values during later stages of mobilization. Mobilized colloids carried a fraction of the cesium along. While transport of cesium in 1 M $NaNO_3$ background was much faster than in 1 mM $NaNO_3$, cesium attached to colloids moved almost unretarded through the sediments. Cesium attached to mobilized colloids was likely associated with high affinity sorption sites on micas and illites.

Introduction

Radioactive and hazardous waste stored at in the underground tanks at the Hanford site, Washington, has leaked into the vadose zone (*1*). Tank waste supernatants consist of solutions of high pH and ionic strength and contain radioactive contaminants such as Cs. When such a waste plume contacts subsurface sediments and migrates through the vadose zone, its ionic strength will decrease, a scenario which can lead to in situ colloid mobilization and transport (*2*−*5*). If strongly sorbing contaminants are present, the leak scenario can also lead to colloid-facilitated contaminant transport (*6*).

In situ mobilization and transport of colloidal material in natural porous media has been demonstrated for various subsurface materials, such as noncalcareous silt loam soil (*4*, *6*), sand soil (*7*), highly weathered aquifer sand (*8*, *9*), and soils at groundwater recharge facilities (*10*). The major factors inducing mobilization and subsequent transport are a change in solution ionic strength and pH; however, pH is often not that important for permanently charged clay minerals (*4*). Concentrations of mobilized particles can be large, up to a few hundreds of milligrams per liter have been reported for laboratory column outflow (*4*). The experimental evidence suggests that, upon disturbance of ionic strength, in situ colloid mobilization can be an important transport mechanism for colloidal particles. If the disturbance of ionic strength occurs in combination with the presence of sorbing contaminants, the mobilized particles can also act as vectors for accelerated contaminant movement (*6*).

A contaminant of major concern at Hanford is radioactive ^{137}Cs. Initially, ^{137}Cs contributed about 40% of the radioactivity present in the tanks (*11*). Presently, ^{137}Cs and ^{90}Sr together constitute about 99% of the tank's radioactivity (*1*). Whereas ^{90}Sr is believed to remain mostly in the sludge of the tanks, ^{137}Cs is contained in the liquid supernatant that can and has leaked out (*1*). Concentrations of ^{137}Cs in the tanks vary considerably. When the leaks occurred, ^{137}Cs concentrations in tanks SX-108, SX-111, and SX-115 are estimated to have ranged between 0.02 and 0.19 mmol/L (*12*). Ionic strength of the tank supernatants is dominated by NaOH and $NaNO_3$; the latter is estimated to reach up to 5 M $NaNO_3$ (*12*).

We hypothesize that during a tank leak at the Hanford Reservation, in situ colloidal particles are initially immobilized because of the high ionic strength of the leaking solutions. At the same time, Cs sorbs only weakly to the sediments due to the high competition of Na ions. As the ionic strength of the solution is decreased by dispersion and dilution, colloids become mobilized, and at the same time, Cs sorbs much stronger to the stationary sediments as well as to the mobile colloids. Colloid-facilitated transport of Cs is likely under such conditions. To test this hypothesis and to quantify the effects, we simulate a tank leak scenario in a saturated laboratory column experiment. The objectives of this study are to determine (1) whether native colloids can be mobilized in situ during a Hanford tank leak and (2) to what extent Cs transport is affected by colloid mobilization.

Materials and Methods

Sediments and Sediment Characterization. Uncontaminated sediments were obtained from the Hanford Reservation, Submarine Site (218-E−12B). The material consists of a pebbly coarse sand belonging to the Hanford Formation, deposited during the cataclysmic events of the Missoula floods. The sediments were taken from a trench wall in January 2000. The sediments are texturally and mineralogically similar to the material underlying the immediate vicinity of the S−SX (single-shell) tank farm at Hanford (personal communication, Bruce N.Bjornstad, September 2001, Pacific Northwest National Laboratories, Richland, WA). The material was air-dried, dry-sieved through a 2-mm square screen, and stored in five-gallon plastic buckets. The pH, measured in a 1:1 w/w water extract, was 8.0.

For particle size analysis, the sediments were treated with 30% w/w H_2O_2 and 0.5 M Na-acetate to remove organic matter and calcium carbonate. For these treatments, samples were placed on a hot plate (65 °C) for 120 min. Samples were then centrifuged at 48 400 g for 120 min, dried at 105 °C, redispersed in a 0.5 g/L Na-hexametaphosphate solution, and wet-sieved through 1-mm and 0.5-mm square sieves. The material passing through the screens was measured with static light scattering (MasterSizer S, Malvern Instruments Ltd., Malvern, UK). The instrument was equipped with reverse Fourier optics and a Helium−Neon laser of 633 nm wavelength. Particle size distribution was obtained by fitting full Mie scattering functions for spheres. The mineralogy of the sand and silt fraction was determined by preparing thin-sections and examination with a petrographic microscope (*13*). For mineralogical analysis of the clay fraction, sediments

* Corresponding author phone: (509)335-1719; fax: (509)335-8674; e-mail: flury@mail.wsu.edu.

10.1021/es025638k CCC: $22.00
Published on Web 11/07/2002

TABLE 1. Experimental Conditions for Column Experiments

column parameters	values
length and diameter	$L = 21.4$ cm, i.d. $= 2.5$ cm
bulk density	1.69 g/cm^3
saturated water content	0.36 cm^3/cm^3
pore volume	37.8 cm^3
flow rate Q	25.8 cm^3/h
water flux J	5.25 cm/h
temperature	20−22 °C
eluent solutions	1000 mM $NaNO_3$, pH 10 (1 mM Na_2CO_3/$NaHCO_3$)
	1 mM $NaNO_3$, pH 10 (0.1 mM Na_2CO_3/$NaHCO_3$)
Cs pulse	0.1 mM $CsNO_3$

were dispersed in deionized water and the size fraction <2 μm was separated by centrifugation. Potassium saturated and air-dried, K-saturated and 550-heated, Mg-saturated and air-dried, and Mg-saturated and glycerol-solvated samples were analyzed as random powder by X-ray diffraction (Philips XRG 3100, Philips Analytical Inc., Mahwah NJ) with Cu−Kα radiation (*14*). Operating conditions for X-ray diffraction were 35kV and 30mA, with scanning at 0.02 degrees 2-theta/sec. The scans were collected using Datascan and processed with Jade (Materials Data, Inc.). Jade was used to smooth and locate peak positions.

Column Experiments. Hanford sediments were packed into a 2.5-cm i.d., 21.4-cm long glass column equipped with Teflon end-pieces (Omnifit, Cambridge, UK). Dry sediments were filled in 1-cm increments under a CO_2 atmosphere into the column, and each increment was then saturated with a 1 M $NaNO_3$ solution by pumping from the bottom before the next increment was added. The strong electrolyte solution kept the fine particles flocculated and allowed a uniform filling of the entire column. After packing, a steady-state flow rate was established using a peristaltic pump (Ismatec IP4, Glattbrugg, Switzerland). All connections and tubings were made of Teflon, except for the peristaltic pump tubing piece, which was of Tygon. A 20 μm pore-size Teflon frit was used at the column inflow end, no frit was used at the outflow end. Column outflow was collected with a fraction collector in 9-mL increments. Four hundred pore volumes of 1 M $NaNO_3$ were initially pumped through the column to equilibrate the material with the electrolyte solution. All eluent solutions were degassed under vacuum, buffered at pH 10 with Na_2CO_3/$NaHCO_3$, and filtered through a 0.1 μm filter (Millipore, polyvinylidene fluoride membrane filter). The ionic strength of the buffer electrolytes was kept at least one order of magnitude smaller than that of the $NaNO_3$ solution. Inflow and outflow pH were monitored periodically to ensure constant pH conditions. Direction of flow during the experiments was from top to bottom. The column was wrapped in aluminum foil to prevent light-induced growth of algae. The foil was periodically removed to visually inspect the column for uniformity of packing and water content during the course of the experiment. Relevant column parameters are summarized in Table 1.

After equilibration of the column with $NaNO_3$, the eluent was changed for about 40 pore volumes to a NaCl solution keeping the same ionic strength and pH. The NaCl was then replaced with a step input of the original $NaNO_3$ to measure the NO_3^- breakthrough. Thirty pore volumes following the $NaNO_3$ input, a 0.1 mM $CsNO_3$ pulse in the same $NaNO_3$ eluent background was introduced. After Cs had eluted from the column, we changed the eluent solution to 1 mM $NaNO_3$ to initiate colloid mobilization. When no more colloids were detected in the outflow, a second Cs pulse was introduced, followed by another NO_3^- breakthrough after initial replacement of $NaNO_3$ with NaCl. The eluent was then changed back to 1 M $NaNO_3$ to obtain a third Cs breakthrough curve. For all Cs breakthrough curves, Cs was added as a pulse in the inflow until the outflow concentration had reached the inflow concentration. Figure 1 shows a synopsis of the column history.

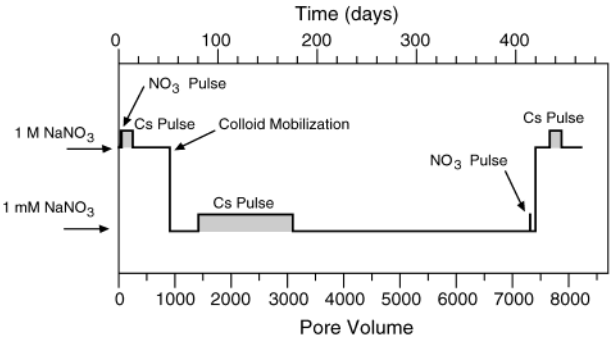

FIGURE 1. Summary of events during the column study.

In summary, the column study consists of a sequence of four experiments: (1) First a Cs breakthrough experiment was conducted in high ionic strength where colloidal material is aggregated and does not move. Due to the presence of micaceous minerals, we expect that a portion of the Cs will not elute and remain inside the column. (2) During the change of ionic strength from high to low, colloidal material will be dispersed and mobilized, and thereby carrying a fraction of the remaining Cs with it. (3) A second Cs breakthrough experiment was measured at low ionic strength, after colloids had eluted from the column. In this phase, no colloids are present in the eluent anymore. (4) Finally a Cs breakthrough experiment was conducted at high ionic strength again, to compare with the initial Cs breakthrough. Again, in this phase, no colloids will be mobile.

Analysis of Nitrate Breakthrough Curves. Column Peclet numbers (Pe) were determined by fitting an analytical solution of the advection-dispersion equation to the conservative tracer breakthrough curve, before and after colloid mobilization following standard procedures (*15*). A Dirichlet boundary condition was employed at the top and a Neumann boundary condition at the bottom of the column. Peclet numbers were estimated using the Levenberg−Marquardt optimization algorithm (*16*).

Colloid Characterization. The outflow samples containing colloidal material were vibrated with a vortex mixer, sonicated for 20 min, and then split in three aliquots. The first aliquot was used to determine colloid concentrations, electrophoretic mobility, and particle morphology. Electrophoretic mobilities were measured with dynamic light scattering using a Zetasizer 3000HSA with a Helium−Neon laser of 633 nm wavelength (Malvern Instruments Ltd., Malvern, UK). For the dynamic light scattering measurements, the background electrolyte concentration used was the same as the one eluted from the column, and the particle concentrations were adjusted to be between 0.1 and 20 mg/L to obtain optimal count rates. The second aliquot was flocculated with a few drops of 1 M $NaNO_3$ and centrifuged at 9200 g for 5 min (this will settle out aggregates with equivalent radii larger than $\sim 7.1 \times 10^{-8}$m). The supernatant was then analyzed for solution phase Cs. The third aliquot was evaporated on a hot plate, and colloids were digested as follows: Colloids were treated overnight with 2 mL of H_2O_2 (30% w/w) at room temperature and then heated to 85 for 2 h. Five mL of aqua regia, consisting of HNO_3 (70%), HCl (37%) and H_2O in a 1:3:1 (w/w/w) ratio, were added, heated on a hot plate to 90 °C, and refluxed for 5 to 6 h. The liquid was then evaporated, and five mL of HNO_3 (5%) was added and stirred with a vortex stirrer. Colloids were allowed to settle and supernatant siphoned off for Cs analysis. It was

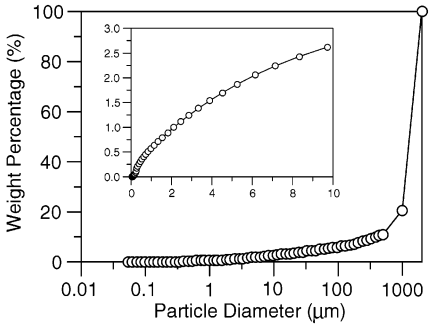

FIGURE 2. Particle size distribution of Hanford sediments used in this study. The inset shows a magnification of the small particle sizes on a linear scale.

assumed that this digestion yields total Cs concentrations in the samples, and using mass balance considerations, concentrations of Cs attached to the colloidal phase were then calculated based on the solution phase concentration from the second aliquot (*6*). The Cs extraction procedure was tested with colloids spiked with known amounts of Cs and a standard soil sample. Cesium recovery of the procedure was between 97 and 103%. For XRD measurements, several samples were combined to obtain sufficient material and analyzed as described above. Insufficient colloidal material was available to measure a complete suite of XRD treatments; only K-saturated and air-dried, K-saturated and heated, and Mg-saturated and glycerol-solvated spectra were determined. Scanning electron microscope (SEM) images were taken with a Hitachi S-570 electron microscope. Colloidal dispersions, containing 0.15% w/w tertbutylamine to reduce surface tension, were added to carbon-coated electron microscopy stubs, evaporated in a laminar-flow hood, gold-coated, and examined with SEM. Particles tended to aggregate during evaporation of the suspensions on the microscopy stubs, and to minimize aggregation, we diluted the suspensions by factors of ten.

Nitrate, Cesium, and Colloid Concentration Analysis. Nitrate and colloid concentrations were measured with a spectrophotometer (HP 8452A, Hewlett-Packard) at a wavelength of 220 and 380 nm, respectively. For colloid measurements, the calibration curve was established with a series of samples that were oven-dried and colloid mass determined gravimetrically. Cesium from the breakthrough curves was measured by atomic emission spectroscopy (Varian 220 Flame Atomic Absorption Spectrometer, Varian Ltd., Mulgrave, Australia) in a 1000 mg/L K background. Cesium concentrations from the colloid mobilization experiment were measured with ICP-MS (Sciex Elan model 250 ICP-MS).

Results and Discussion

Sediment Characterization. The Hanford sediments used are very coarse, with 89% of the mass larger than 0.5 mm and only 1% smaller than 2 μm (Figure 2). The sand and silt fractions are dominated by quartz, amphibole, plagioclase, K-feldspar, mica, and magnetite. Among the micas, both muscovite and biotite are common. The clay-size fraction consists mainly of chlorite, smectite, vermiculite, kaolinite, illite, and quartz.

Column Hydrodynamics. Colloid mobilization, induced by the change in ionic strength, can potentially lead to an alteration of the hydrodynamic properties of the porous medium. The column hydrodynamics was assessed by a series of conservative tracer breakthrough experiments. The results showed that the hydrodynamics of the column did not change during the course of the experiment. The mobilization and elution of colloidal material did not significantly affect the

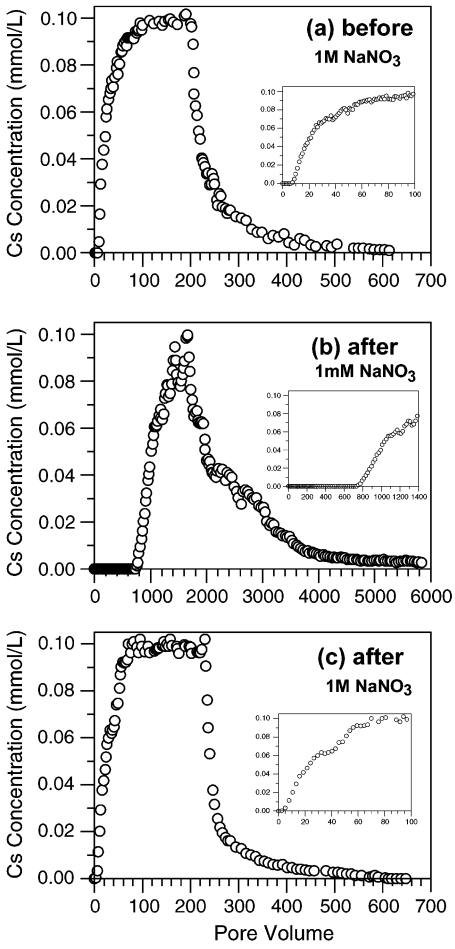

FIGURE 3. Cesium breakthrough curves in Hanford sediments in absence of colloid-facilitated transport. (a) Before colloid mobilization (1 M $NaNO_3$), (b) after colloid mobilization (1 mM $NaNO_3$), (c) after colloid mobilization (1 M $NaNO_3$). Insets show detail from the initial part of the breakthrough. In all cases, colloid concentrations in the eluent were below the analytical detection limit.

column Peclet number (Table 2), and the tracer breakthrough curves were not distinguishable. The hydrodynamic dispersion in our system appears to be determined largely by the coarse sediment material.

Cesium Transport. We are expecting two counteracting phenomena governing the transport of Cs in our column experiment. At the high ionic strength, Cs sorption to Hanford sediments is suppressed because of competition with Na for sorption sites. At the low ionic strength, Cs sorbs more strongly, but the sediment matrix has lost some of its fine material during the colloid mobilization, and consequently Cs sorption will decrease because fewer sorption sites are available. Which effect will dominate is difficult to assess a priori. The experiments showed that the ionic strength effect clearly dominated the transport of Cs. At 1 M $NaNO_3$, Cs breakthrough, defined as $C/C_0 = 0.5$, where C_0 is the concentration of the Cs pulse, occurred after 25 pore volumes, whereas at 1 mM $NaNO_3$, Cs breakthrough occurred after 950 pore volumes (Figure 3). The two breakthrough curves differed not only in breakthrough time but also in shape. Compared to the 1 M $NaNO_3$ case, the 1 mM $NaNO_3$ breakthrough curve has a steeper breakthrough front and a more pronounced tailing. This indicates that the sorption process is more nonlinear at the low ionic strength than at the high ionc strengths. The Cs breakthrough in 1 M $NaNO_3$ after colloid mobilization (Figure 3c) is almost identical to the Cs breakthrough in 1 M $NaNO_3$ before colloid mobilization. However, there is somewhat less tailing in the desorption

TABLE 2. Peclet Numbers and Experimental Cesium Mass Recoveries

parameters	units	1 M $NaNO_3$	1 mM $NaNO_3$	1 M $NaNO_3$
colloids eluted		no	yes	yes
Peclet no.[a] Pe = VL/D		76.9 ± 9.8	67.7 ± 5.7	67.7 ± 6.2
exptl mass recovery	%	99.43	98.24	97.57

[a] Column Peclet number based on pore water velocity V, column length L, and hydrodynamic dispersion coefficient D; determined from NO_3 breakthrough curves.

part of the breakthrough curve after colloids have eluted from the column.

The mass recovery indicates that most of the Cs was eluted from the columns (Table 2). The mass recovery of the second Cs pulse in 1 M $NaNO_3$ was likely the least accurate because the measured high concentration values were variable.

Colloid Mobilization. Colloids were mobilized and transported through the column as the ionic strength was lowered from 1000 to 1 mM $NaNO_3$. The breakthrough occurred one pore volume after change of the inflow solution, basically following the normality front (Figure 4a). It is expected that the pH of the eluent solution will increase during the displacement of the high with the low ionic strength solution (*17*), but because of the pH buffering, the equilibrium pH should be attained again within a few pore volumes (*4*).

The peak colloid concentration was reached at five pore volumes, and colloids kept eluting from the column for about 250 pore volumes, after which the concentrations fell below the analytical detection limit. The concentrations of colloidal particles in the outflow reached up to 900 mg/L. Obviously, the maximum concentrations observed are a function of the solution composition, in particular the ionic strength and valence of the electrolytes, but, nevertheless, values in the same order of magnitude have been reported from other in situ colloid mobilization experiments in natural porous media (*4*, *18*−*20*). These colloid concentrations are 2 to 4 orders of magnitude larger than concentrations found in geochemically stable subsurface systems; however, it is known that during geochemical disturbance, colloid concentrations can increase several orders of magnitude compared to the stable geochemical conditions (*2*). Whereas the shape of the colloid breakthrough curve shows a sharp peak, the elution portion shows a pronounced tailing and indicates two different rates of colloid release (Figure 4a,b).

The electrophoretic mobility of the eluted particles was initially constant at −3 (μm/s)(V/cm) (Figure 4c). After about 100 pore volumes, the electrophoretic mobilities became more variable and increased to −2.5 to −1.8 (μm/s)(V/cm). The colloid concentrations at that time were already small, i.e., less than 10 mg/L. We believe that the change in electrophoretic mobility is caused because the most mobile colloids (with the most negative electrophoretic mobility) are eluted first and the colloids with the less negative electrophoretic mobility lag behind. After 300 pore volumes, colloid concentrations were so small that no electrophoretic mobility measurements were possible.

The SEM images indicated that the colloids were polydisperse and of irregular shape and, interestingly, also showed that relatively large particles (up to 15 μm diameter) were eluted from the column (Figure 5). Individual particle diameters determined with SEM ranged from 0.2 to 15 μm. In the SEM images, individual smaller particles were often forming larger aggregates, which probably formed during the drying process on the SEM stubs. Larger aggregates consisted of crystalline particles resembling kaolinite and illite (upper left in Figure 5), whereas smaller aggregates often appeared to consist of smectite (lower left in Figure 5). The

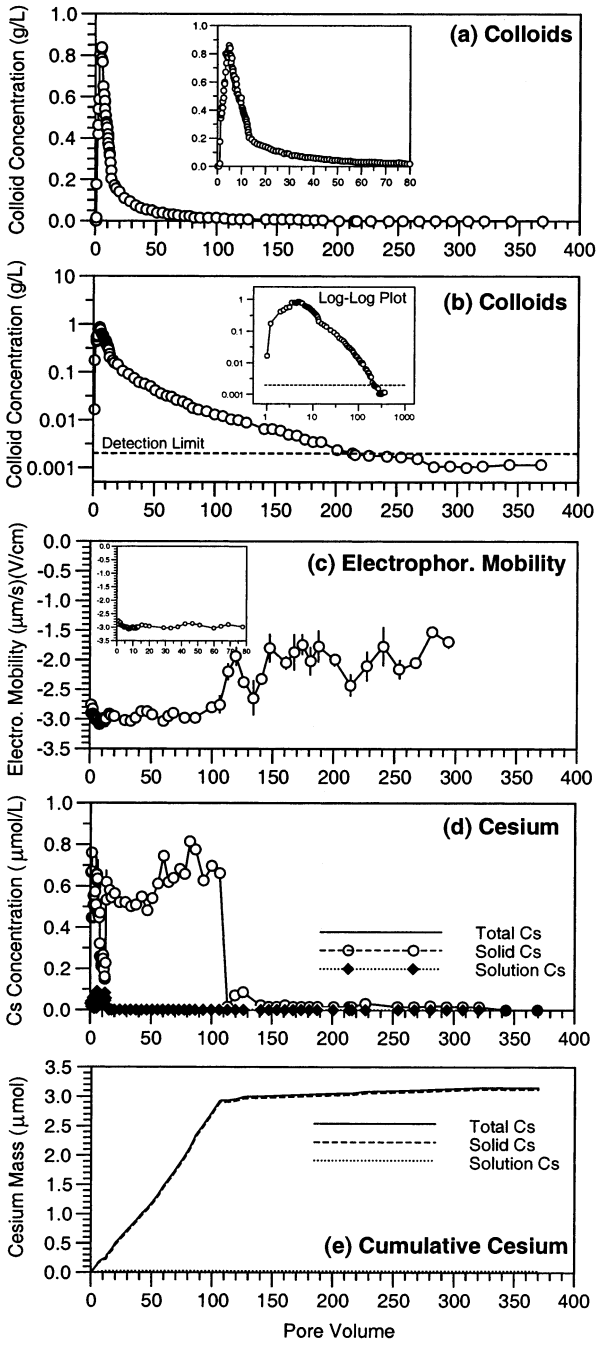

FIGURE 4. Column outflow after eluent change from 1 M to 1 mM $NaNO_3$. The pore volume axis starts when the ionic strength of the inflow was changed. (a) Colloid concentration breakthrough curve, (b) colloid breakthrough curve in semi-log scale, (c) electrophoretic mobility measured at pH 10 and 1 mM $NaNO_3$, (d) Cs concentration breakthrough, and (e) cumulative Cs breakthrough. The vertical bars in (c) indicate ± one standard deviation. The insets show a closeup of the breakthrough portion.

SEM analysis did not show any systematic shape and size pattern as a function of pore volume.

The colloids mobilized were identified as kaolinite, quartz, mica-vermiculite-illite, chlorite, and smectite (Figure 6). The smectite was identified with the Mg-saturated, glycerol-solvated samples. The mineralogical composition of the mobilized colloids is consistent with the composition of the <2 μm-particle fraction of the sediments and with published analyses of sediments from the Hanford formation (*11*). There was no separation of mineral types occurring during the

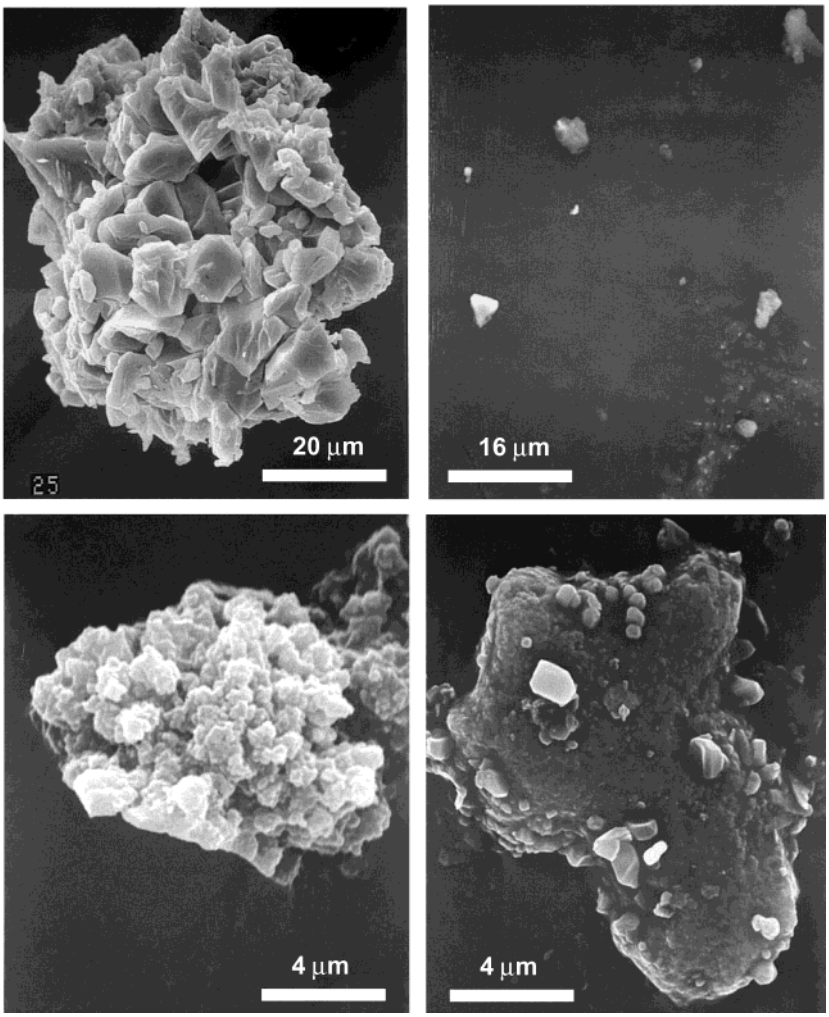

FIGURE 5. Representative SEM images of colloids eluted from the column. Images were taken at 20 kV. Upper right image is taken from a diluted sample to minimize aggregation.

mobilization event, although there appears to be less smectite and chlorite in the later stages of the colloid mobilization. It is noteworthy that minerals usually accounted to the silt and sand fraction, like mica and quartz, were eluted along with the clay minerals kaolinite, smectite, illite, and chlorite.

Colloid-Facilitated Cs Transport. The first Cs pulse introduced at 1 M $NaNO_3$ was eluted for the most part (99.43%); however some Cs still remained in the column. Cesium is known to sorb to high and low affinity sites in sediments such as ours (*11*, *21*). High affinity sorption sites are frayed edge sites and interlayer sites of nonexpansible 2:1 phyllosilicates, such as micas and illites (*22*, *23*). The low-affinity sites are mainly the planar surfaces of phyllosilicate clay minerals. Iron oxyhydroxides and quartz do not sorb Cs to a significant amount (*23*), nor does organic matter (*22*). It is likely, during the Cs breakthrough in 1 M $NaNO_3$, the Cs had saturated all high- and low-affinity sorption sites during the adsorption part, but during the desorption part, only the Cs at the low-affinity sorption sites has been desorbed via cation exchange with Na. In addition, Cs desorption from high-affinity sites is much slower than from the low-affinity sites (*24*, 25). Therefore, some Cs at high-affinity sites will have remained in the column, likely attached to micas and nonexpansible clay minerals. Indeed, after change of the ionic strength to induce colloid mobilization, the eluted colloids carried some Cs with them, and the Cs was associated mostly with the colloidal phase (Figure 4d,e). Total concentrations of Cs in the outflow varied between 0.5 and 0.8 μmol/L and dropped to below 0.03 μmol/L after 110 pore volumes. There is a sudden drop in colloid-associated Cs concentrations after 110 pore volumes, which coincides with an increase of electrophoretic mobility of colloidal particles. Attempts to identify a possible change in mineralogy of the colloids associated with this drop failed because of insufficient amount of colloidal material available for XRD.

Some Cs was detected in the solution phase, but the concentrations were small (<0.01 μmol/L). The only significant concentrations in the solution phase were measured within the first 15 pore volumes following colloid elution when solution phase concentrations reached up to 0.1 μmol/L. The bulk portion of the Cs was associated with the colloidal phase. Based on studies on contaminated sediments from the Hanford Site, it is likely that the Cs was mainly carried by biotite and to a lesser degree by vermiculite (*11*); however, we have not specifically identified the Cs-carrying phases in our experiment.

We calculated the mass balance of Cs for the mobilization experiment based on the concentrations measurements in the outflow (Figure 7). Most of the Cs introduced into the column was eluted during the Cs breakthrough experiment (1 M $NaNO_3$), accounting to 99.43% of the Cs mass. After the change in ionic strength, an additional 0.432% of the Cs was eluted. The colloid-associated Cs amounted to 0.428%. A negligible amount of Cs (0.004%) was detected in the solution phase during the colloid mobilization experiment. Based on the mass balance calculation, the 0.428% of colloid-associated Cs might not seem like much; however, considering the portion of Cs remaining inside the column after the first Cs

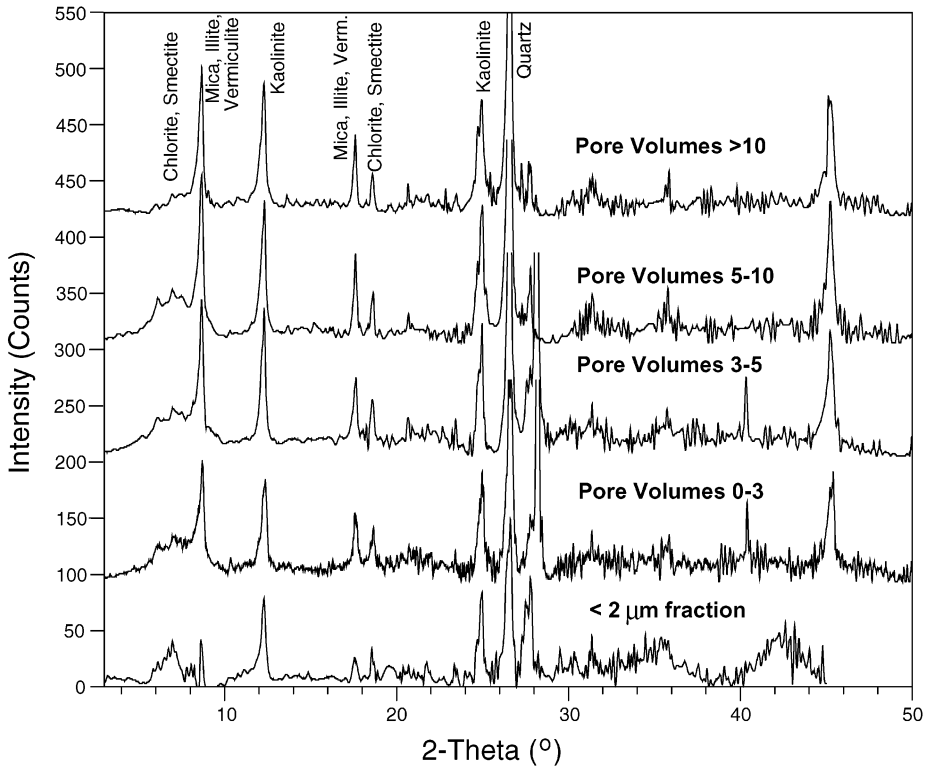

FIGURE 6. X-ray diffraction patterns (K-saturated, air-dried) of <2 μm-fraction of the sediments (bottom curve) and the mobilized colloids for different portions of the breakthrough curve (four upper curves).

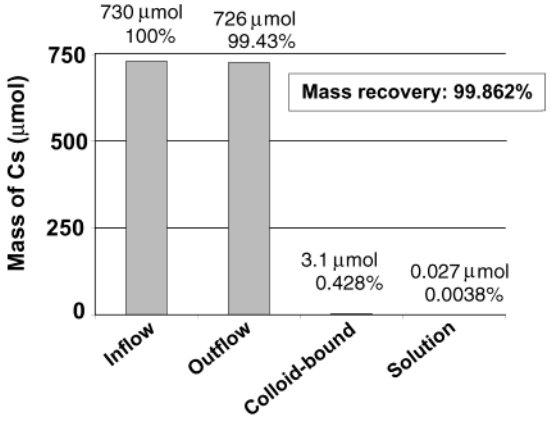

FIGURE 7. Mass balance calculations from Cs breakthrough curves and colloid mobilization experiment.

breakthrough curve, the eluted colloid-associated Cs accounts for 75.09% of the Cs remaining in the column. A considerable amount of the Cs remaining in the column was therefore mobilized via colloidal particles.

The amount of Cs mobilized with colloids was 3.1 μmol or, related to the mass of sediments in the column, 5.59×10^{-8} mol/g (Figure 7). This number is similar to the concentration of poorly exchangeable Cs, reported as 3.45×10^{-8} mol/g, calculated from batch sorption studies with Hanford sediments under high Na background (5 M $NaNO_3$) (*21*). Zachara et al. (*21*) also estimated the concentration of frayed edge sites using the AgTU-method, which, at 4.92×10^{-8} mol/g, was similar to the concentration of poorly exchangeable Cs. Considering the experimental errors involved in the mass balance calculations and the variability of Hanford sediments, this agreement is remarkable. It is therefore plausible that the Cs attached to the mobilized colloids was mainly poorly exchangeable and associated with frayed edge sites.

Implications for Radionuclide Transport. The results of this column experiment can be applied to the situation of Hanford tank leakage. Chemical conditions in our experiment were chosen to mimic a tank leak at Hanford. It is known that colloid mobilization is dependent on the water flow rate (*7*, *19*). The flow rate in our experiment (1.26 m/d) is well within the range of saturated and unsaturated hydraulic conductivities measured in sediments from the Hanford formation (*26*). We have demonstrated that in situ colloid mobilization from Hanford sediments is possible and that the mobilized colloids can facilitate the transport of sorbed Cs. Although Cs is mobile at high ionic strength, the mobility of colloid-bound Cs is much better. Colloid-bound Cs traveled almost unretarded through our column. The colloids mobilized from the sediments consisted of minerals that are known to sorb Cs strongly, including micas and illites, and which are also known to retain some of the ^{137}Cs that has leaked from the waste tanks. At this time, however, we do not know how far the mobilized colloidal material will travel through the vadose zone and what the conditions would be under unsaturated flow.

Acknowledgments

This work was supported by the Environmental Management Science Program, U.S. Department of Energy under contract DE-FG07-99ER62882, Project Officers Drs. Frank Wobber and Chester Miller. We thank Jeff Boyle (Washington State University, WSU) for his help with XRD and cesium measurements, the Electron Microscopy Center at WSU for use of their facility, and John Zachara and Jeff Serne (Pacific Northwest National Laboratory) for providing us with the Hanford sediments. We thank three anonymous reviewers for helpful suggestions.

Literature Cited

(1) Gephart, R. E.; Lundgren, R. E. *Hanford Tank Cleanup: A Guide to Understanding the Technical Issues*, 4th ed.; Battelle Press: Columbus, 1998.

(2) McCarthy, J. F.; Degueldre, C. In *Environment Particles*; Buffle, J., van Leeuwen, H., Eds.; Lewis Publisher: Boca Raton, FL, 1993; Vol. II, pp 247−315.
(3) Ryan, J. N.; Elimelech, M. *Colloids Surf.* **1996**, *107*, 1−56.
(4) Grolimund, D.; Borkovec, M. *Environ. Sci. Technol.* **1999**, *33*, 4054−4060.
(5) Kretzschmar, R.; Borkovec, M.; Grolimund, D.; Elimelech, M. *Adv. Agron.* **1999**, *66*, 121−193.
(6) Grolimund, D.; Borkovec, M.; Barmettler, K.; Sticher, H. *Environ. Sci. Technol.* **1996**, *30*, 3118−3123.
(7) Kaplan, D. I.; Bertsch, P. M.; Adriano, D. C.; Miller, W. P. *Environ. Sci. Technol.* **1993**, *27*, 1193−1200.
(8) Seaman, J. C.; Bertsch, P. M.; Miller, W. P. *Environ. Sci. Technol.* **1995**, *29*, 1808−1815.
(9) Seaman, J. C.; Bertsch, P. M.; Strom, R. N. *Environ. Sci. Technol.* **1997**, *31*, 2782−2790.
(10) Nightingale, H. I.; Bianchi, W. C. *Ground Water* **1977**, *15*, 146−152.
(11) McKinley, J. P.; Zeissler, C. J.; Zachara, J. M.; Serne, R. J.; Lindstrom, R. M.; Schaef, H. T.; Orr, R. D. *Environ. Sci. Technol.* **2001**, *35*, 3433−3441.
(12) Serne, R. J.; Zachara, J. M.; Burke, D. S. *Chemical Information on Tank Supernatants, Cs Adsorption from Tank Liquids onto Hanford Sediments, and Field Observations of Cs Migration from Past Tank Leaks*; Pacific Northwest National Laboratory, PNNL-11495/UC-510: Richland, WA, 1998.
(13) Cady, J. G.; Wilding, L. P.; Drees, L. R. *In Methods of Soil Analysis. Part 1. Physical and Mineralogical Methods*; Klute, A., Ed.; American Society of Agronomy: Madison, Wisconsin, 1986; 2nd ed., pp 185−218.
(14) Whittig, L. D.; Allardice, W. R. *In Methods of Soil Analysis. Part 1. Physical and Mineralogical Methods*; Klute, A., Ed.; American Society of Agronomy: Madison, Wisconsin, 1986; 2nd ed., pp 331−362.
(15) Fortin, J.; Flury, M.; Jury, W. A.; Streck, T. *J. Contam. Hydrol.* **1997**, *25*, 219−234.
(16) Press, W. H.; Teukolsky, S. A.; Vetterling, W. T.; Flannery, B. P. *Numerical Recipes. The Art of Scientific Computing*, 2nd ed.; Cambridge University Press: Cambridge, 1992.
(17) Scheidegger, A.; Bürgisser, C. S.; Borkovec, M.; Sticher, H.; Meeussen, H.; van Riemsdijk, W. *Water Resour. Res.* **1994**, *30*, 2937−2944.
(18) Jacobsen, O. H.; Moldrup, P.; Larson, C.; Konnerup, L.; Petersen, L. W. *J. Hydrol.* (Amsterdam) **1997**, *196*, 185−203.
(19) Ryan, J. N.; Illangasekare, T. H.; Litaor, M. I.; Shannon, R. *Environ. Sci. Technol.* **1998**, *32*, 476−482.
(20) Grolimund, D.; Elimelech, M.;Borkovec, M.; Barmettler, K.; Kretzschmar, R.; Sticher, H. *Environ. Sci. Technol.* **1998**, *32*, 3562−3569.
(21) Zachara, J. M.; Smith, S. C.; Liu, C.; McKinley, J. P.; Serne, R. J.; Gassman, P. L. *Geochim. Cosmochim. Acta* **2002**, *66*, 193−211.
(22) Cremers, A.; Elsen, A.; de Preter, P.; Maes, A. *Nature* **1988**, *335*, 247−249.
(23) Cornell, R. M. *J. Radioanal. Nuclear Chem.* **1993**, *171*, 483−500.
(24) Comans, R. N. J.; Haller, M.; de Preter, P. *Geochim. Cosmochim. Acta* **1991**, *55*, 433 −440.
(25) Comans, R. N. J.; Hockley, D. E. *Geochim. Cosmochim. Acta* **1992**, *56*, 1157−1164.
(26) Khaleed, R.; Freeman, E. J. *Variability and Scaling of Hydraulic Properties for 200 Area Soils, Hanford Site*; Westinghouse Hanford Company, WHC-EP-0883: Richland, WA, 1995.

Received for review March 9, 2002. Revised manuscript received July 26, 2002. Accepted September 17, 2002.

ES025638K